On the Spectral Moments of Non-WSSUS Mobile-to-Mobile Double-Rayleigh Fading Channels

J. J. Jaime-Rodríguez, C. A. Gutiérrez
Faculty of Science,
Uiversidad Autónoma de San Luis Potosí
Av. Dr. Salvador Nava Martínez S/N,
Zona Universitaria,
San Luis Potosí 78290, México
Emails: j.j.jaime@ieee.org, cagutierrez@ieee.org

Matthias Pätzold, Alireza Borhani
Faculty of Engineering and Science
University of Agder
P.O. Box 509, 4898 Grimstad, Norway
Emails: matthias.paetzold@uia.no, alireza.borhani@uia.no

Abstract—This paper deals with the mathematical analysis of the spectral moments of non-wide-sense-stationary uncorrelated-scattering (non-WSSUS) mobile-to-mobile (M2M) double-Rayleigh fading channels. The point of departure is a recently proposed geometry-based statistical model (GBSM) for M2M double-Rayleigh fading channels from which general analytical expressions are derived for the average Doppler shift, Doppler spread, average delay, and delay spread. Closed-form solutions of such expressions are presented for the particular case of the geometrical two-rings scattering model. The obtained results indicate that the average Doppler shift and Doppler spread are directly influenced by not only the carrier frequency, but also the bandwidth of the communication system. A consistency analysis is carried out to assess the physical soundness of the reference channel model. The results show that the channel model fulfills all the consistency criteria pertaining to the spectral moments. The analysis presented here can be used as a guideline for the statistical characterization of non-WSSUS time- and frequency-selective M2M fading channels.

I. INTRODUCTION

Government agencies in conjunction with automotive companies are promoting the development and implementation of intelligent transportation systems (ITS) as a technological solution to reduce road accidents and increase transportation efficiency. One of the main challenges in the development of ITS is the integration of mobile-to-mobile (M2M) communication technologies allowing for reliable real time communications among vehicles. This is not a trivial task, because the propagation conditions change rapidly in M2M communications, as both the transmitter (T_X) and receiver (R_X) are

moving at high vehicular speeds. For this reason, the wide-sense-stationary uncorrelated-scattering (WSSUS) assumption that has widely been accepted for the statistical characterization of fixed-to-mobile (F2M) fading channels [1], [2] is not suitable for the modeling of M2M fading channels. Furthermore, empirical data obtained from measurement campaigns [3]–[6] indicate that the signals propagating through M2M channels are subject to worse-than-Rayleigh fading, e.g., double-Rayleigh fading. Thus, the formulation of new statistical channel models capturing the non-stationary characteristics of real-world time-frequency (TF) selective M2M channels has become indispensable.

In this context, a novel geometry-based statistical model (GBSM) for TF selective non-WSSUS M2M double-Rayleigh fading channels was recently presented in [7]. This model was formulated considering a generic non-regular geometrical configuration of the propagation area. It provides a flexible framework for the analysis of the channel's non-stationarities caused by the time-varying (TV) propagation delays. A comprehensive analysis of the probability density function (PDF) of the envelope and phase, the four-dimensional (4D) TF correlation function (CF), the TF-dependent power delay profile (PDP), and the TF-dependent Doppler spectrum of this GBSM were investigated in [7]. In this paper, we complete the work of [7], [8] by providing a through mathematical analysis of the spectral moments of such types of GBSMs for non-WSSUS M2M double-Rayleigh fading channels. Specifically, we derive general expressions for the average delay, delay spread, average Doppler shift, and Doppler spread by considering an arbitrary geometrical configuration of the propagation scenario. In addition, we present closed-form solutions of such expressions for the particular case of the two-rings scattering model [9]. The obtained expressions show that

the average delay and the delay spread are TV quantities. On the other hand, the average Doppler shift and the Doppler spread are shown to be frequency-varying quantities. Our results also show that the average Doppler shift and the Doppler spread are directly influenced by not only the carrier frequency, but also by the frequency bandwidth of the communication system. In order to validate the obtained results, following the metrics introduced in [10], we perform a consistency analysis of the channel model. As we will see, our reference model in [7] fulfills all the conditions defined to be considered as consistent w.r.t. the spectral moments.

The paper is structured as follows. The reference model is introduced in Section II. The computation of the spectral moments and the analysis of consistency are the topics of Section III. Some illustrative numerical results are presented in Section IV. Finally, our conclusions are summarized in Section V.

II. THE REFERENCE CHANNEL MODEL

A. Description of the M2M Propagation Scenario

The geometrical configuration of the propagation scenario considered in [7] is shown in Fig. 1. It is assumed that the transmitted signal reaches R_X (black square) by means of a double interaction with fixed interfering objects (IOs) randomly located around the MSs. Both T_X (black triangle) and R_X are moving at constant speeds over linear trajectories. The transmitted signal interacts first with a set $\mathbb{S}_T$ of L IOs placed in the vicinity of T_X. As a result of such an interaction, L copies or echoes of the transmitted signal reach a second set $\mathbb{S}_R$ of M IOs which are surrounding R_X. Hence, $L \times M$ copies of the transmitted signal are generated, which impinge on the R_X antenna and combine with one another.

When the MSs start a communication at $t = t_0$, as illustrated in Fig. 1, the positions of T_X and R_X are described by the time-invariant vectors $\mathbf{O}_T$ and $\mathbf{O}_R$, respectively. The distance between T_X and R_X is denoted by D. The symbols $\mathbf{v}_T$ and $\mathbf{v}_R$ designate the velocity vectors of T_X and R_X, respectively. The L IOs in the set $\mathbb{S}_T$ appear as white dots, while black dots are the M IOs in $\mathbb{S}_R$. The lth IO in $\mathbb{S}_k$ is represented as S_l^k for $l \in \{1, 2, ..., \text{card}(\mathbb{S}_k)\}$ and $k \in \{T, R\}$, and the time-invariant vectors $\hat{\mathbf{p}}_l^k$ stand for the position of S_l^k w.r.t. the fixed reference point $\mathbf{O}_k$. The instantaneous position of S_ℓ^T as seen from the moving T_X, is denoted by the TV vector $\mathbf{p}_\ell^T(t)$. In the same way, $\mathbf{p}_m^R(t)$ indicates the instantaneous position of S_m^R, as seen from the moving R_X. Furthermore, the position of S_m^R w.r.t. S_ℓ^T is given by the time-invariant vector $\mathbf{p}_{\ell,m}^S$. The time-invariant vectors $\mathbf{u}_\ell^T$, $\mathbf{u}_{\ell,m}^S$, and $\mathbf{u}_m^R$ are unit vectors that point at the propagation direction of the waves that travel from T_X to S_ℓ^T, from S_ℓ^T to S_m^R, and from S_m^R to R_X, respectively.
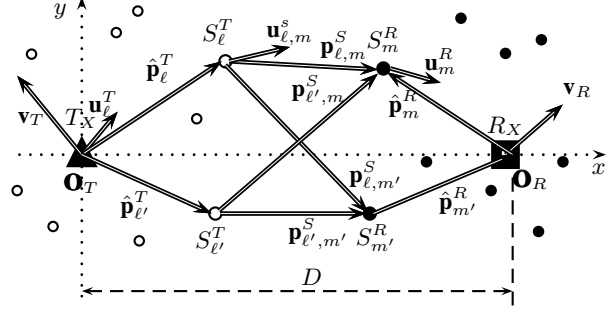

Fig. 1. M2M propagation scenario at time $t = t_0$.

B. Mathematical Model of the Channel Transfer Function

The channel transfer function is modeled in [7] in the equivalent complex baseband at time $t_0 = 0$ as

$$
\begin{aligned}
H(t; f) &= \Pi_{T_0}(t) \sum_{\ell=1}^{L} \sum_{m=1}^{M} g_\ell^T \, g_m^R \\
&\times \exp\left\{-j\left[\theta_\ell^T + \theta_m^R\right]\right\} \\
&\times \exp\left\{-j2\pi\left(f_c + f\right)\tau_{\ell,m}(t)\right\} \quad (1)
\end{aligned}
$$

where $j^2 = -1$, f denotes the frequency variable, g_l^k and θ_l^k stand for the gain and phase shift, respectively, caused by the interaction of the transmitted signal with S_l^k for $l \in \{1, 2, ..., \text{card}(\mathbb{S}_k)\}$ and $k \in \{T, R\}$. The carrier frequency is $f_c = C/\lambda$, where C stands for the speed of light, and λ is the transmitted signal's wavelength. Furthermore, $\Pi_{T_0}(t) = 1$ for $0 \leq t \leq T_0$, and $\Pi_{T_0}(t) = 0$ elsewhere. The function $\Pi_{T_0}(t)$ denotes a rectangular windowing function that has been introduced to constrain $H(t; f)$ within an interval of length T_0, where the plane wave propagation model is valid. In addition, the TV propagation delays $\tau_{\ell,m}(t)$ are given as [7]

$$
\begin{aligned}
\tau_{\ell,m}(t) &= \frac{\| \hat{\mathbf{p}}_\ell^T \| + \| \mathbf{p}_{\ell,m}^S \| + \| \hat{\mathbf{p}}_m^R \|}{C} \\
&\quad -t\frac{f_{\ell,m}^D(f)}{f_c + f} \quad (2)
\end{aligned}
$$

where $\| \cdot \|$ denotes the Euclidean norm. According to [7], the Doppler shift $f_{\ell,m}^D(f)$, which is caused by the combined movement of T_X and R_X, is given by

$$
f_{\ell,m}^D(f) = f_T(\phi_\ell^T) + f_R(\phi_m^R) \quad (3)
$$

where ϕ_ℓ^T represents the angle of departure (AOD) of the wave that interacts with the ℓth IO of the set $\mathbb{S}_T$, and ϕ_m^R denotes the angle of arrival (AOA) of the signal that arrives at R_X via the mth IO of the set $\mathbb{S}_R$. The AOD ϕ_ℓ^T and the AOA ϕ_m^R are modeled by random variables characterized by PDFs $p_\phi^T(\phi_\ell^T)$ and $p_\phi^R(\phi_m^R)$, respectively. In addition,

$$
f_k(\phi_l^k) = f_{\max}^k \cos(\phi_l^k - \gamma_k), \quad k \in \{T, R\} \quad (4)
$$

$$R_H(t, f; \Delta t, \Delta f) = \sigma_H^2 \Upsilon(t, \Delta t) \int\limits_{-\pi}^{\pi} \int\limits_{-\pi}^{\pi} \exp \left\{ j2\pi \left[\Delta t \left(f_T(\phi_\ell^T) + f_R(\phi_m^R) \right) \right. \right.$$
$$\left. \left. - \Delta f \left(\frac{G_T(\phi_T) + G_S(\phi_T, \phi_R) + G_R(\phi_R)}{C} - t \left(\frac{f_T(\phi_\ell^T) + f_R(\phi_m^R)}{f_c + f} \right) \right) \right] \right\}$$
$$\times p_\phi^T(\phi_T) p_\phi^R(\phi_R) d\phi_T d\phi_R \tag{7}$$

where γ_k is the angle representing the direction of motion of the T_X ($k = T$) and R_X ($k = R$) for $l \in \{\ell, m\}$. In turn, $f_{\max}^k$ is the maximum Doppler frequency shift due to the speed of T_X ($k = T$) and R_X ($k = R$), which is given as

$$f_{\max}^k = \frac{v_k}{\lambda} \left(\frac{f_c + f}{f_c} \right). \tag{5}$$

The speed of T_X and R_X is denoted by v_k for $k \in \{T, R\}$. Furthermore, the path lengths $\| \mathbf{p}_{\ell,m}^S \|$, $\| \hat{\mathbf{p}}_\ell^T \|$, and $\| \hat{\mathbf{p}}_m^R \|$ are modeled as functions of the AODs and AOAs as follows $\| \mathbf{p}_{\ell,m}^S \| = G_S(\phi_\ell^T, \phi_m^R)$, $\| \hat{\mathbf{p}}_\ell^T \| = G_T(\phi_\ell^T)$, and $\| \hat{\mathbf{p}}_m^R \| = G_R(\phi_m^R)$. Thereby, we can rewrite the TV propagation delays as

$$\tau_{\ell,m}(t) = \frac{G_T(\phi_\ell^T) + G_S(\phi_\ell^T, \phi_m^R) + G_R(\phi_m^R)}{C}$$
$$- t \frac{f_T(\phi_\ell^T) + f_R(\phi_m^R)}{f_c + f}. \tag{6}$$

It is shown in [7] that the 4D TF-CF of the channel transfer function presented in (1) is given as in (7) at the top of next page, where $\Upsilon(t, \Delta t) = \Pi_{T_0}(t) \cdot \Pi_{T_0}(t - \Delta t)$, and σ_H^2 is the average power of the channel.

III. SPECTRAL MOMENTS AND ANALYSIS OF CONSISTENCY

A. Spectral Moments

The frequency-varying (FV) average Doppler shift $B_\nu^{(1)}(f)$ and the FV Doppler spread $B_\nu^{(2)}(f)$ of the channel transfer function $H(t; f)$ in (1) can be computed from the Doppler shift $f_{\ell,m}^D(f)$ in (3) as follows [10]:

$$B_\nu^{(1)}(f) = \frac{\sum_{\ell=1}^{L} \sum_{m=1}^{M} \left[g_\ell^T g_m^R \right]^2 f_{\ell,m}^D(f)}{\sum_{\ell=1}^{L} \sum_{m=1}^{M} \left[g_\ell^T g_m^R \right]^2} \tag{8}$$

$$B_\nu^{(2)}(f) = \sqrt{\frac{\sum_{\ell=1}^{L} \sum_{m=1}^{M} \left[g_\ell^T g_m^R f_{\ell,m}^D(f) \right]^2}{\sum_{\ell=1}^{L} \sum_{m=1}^{M} \left[g_\ell^T g_m^R \right]^2} - \left(B_\nu^{(1)}(f) \right)^2}. \tag{9}$$

After substituting (3) into (8) and (9), and knowing from [7] that $\sum_{\ell=1}^{L} \sum_{m=1}^{M} E \left\{ \left(g_\ell^T \right)^2 \right\} E \left\{ \left(g_m^R \right)^2 \right\} = \sigma_H^2$, where $E \{\cdot\}$ denotes the expectation operator, we obtain—after straightforward algebraic manipulations and invoking the expected value theorem—the general expressions.

$$B_\nu^{(1)}(f) = \int\limits_{-\pi}^{\pi} \int\limits_{-\pi}^{\pi} f^D(f) p_\phi^T(\phi_T) p_\phi^R(\phi_R) d\phi_T d\phi_R \tag{10}$$

$$B_\nu^{(2)}(f) = \left\{ \int\limits_{-\pi}^{\pi} \int\limits_{-\pi}^{\pi} \left[f^D(f) \right]^2 p_\phi^T(\phi_T) p_\phi^R(\phi_R) d\phi_T d\phi_R \right.$$
$$\left. - \left[B_\nu^{(1)}(f) \right]^2 \right\}^{1/2}. \tag{11}$$

The TV average delay $B_\tau^{(1)}(t)$ and the TV delay spread $B_\tau^{(2)}(t)$ are equal to right-hand side of (8) and (9), respectively, if we replace there $f_{\ell,m}^D(f)$ by $\tau_{\ell,m}(t)$, and if we use $B_\tau^{(1)}(t)$ in place of $B_\nu^{(1)}(f)$ in (9). Substituting the TV propagation delay $\tau_{\ell,m}(t)$ according to (6) into the *analogous* versions of (8) and (9), we obtain two expressions that have the same form as (10) and (11), but with t instead of f, τ instead of ν, and $\tau(t)$ instead of $f^D(f)$. The results are not presented explicitly due to space limitations.

An alternative for computing the FV average Doppler shift $B_{R_H}^{(1)}(f)$ and the FV Doppler spread $B_{R_H}^{(2)}(f)$ of the channel transfer function $H(t; f)$ in (1), is to use the TF-CF $R_H(t, f; \Delta t, \Delta f)$ in (7). According to [10], $B_{R_H}^{(1)}(f)$ and $B_{R_H}^{(2)}(f)$ are given by

$$B_{R_H}^{(1)}(f) = \frac{1}{2\pi j} \left. \frac{\dot{R}_H(0, f; \Delta t, 0)}{R_H(0, f; \Delta t, 0)} \right|_{\Delta t = 0} \tag{12}$$

$$B_{R_H}^{(2)}(f) = \frac{1}{2\pi} \left[\left(\frac{\dot{R}_H(0, f; \Delta t, 0)}{R_H(0, f; \Delta t, 0)} \right)^2 \right.$$
$$\left. - \frac{\ddot{R}_H(0, f; \Delta t, 0)}{R_H(0, f; \Delta t, 0)} \right]^{\frac{1}{2}} \Bigg|_{\Delta t = 0} \tag{13}$$

By analogous eq. $(\cdot)$, we mean that in eq. $(\cdot)$ all frequency variables are replaced by the dual temporal variables (see Sec. III-A).

where $\dot{R}_H(0, f; \Delta t, 0)$ and $\ddot{R}_H(0, f; \Delta t, 0)$ are the first and second derivative of $R_H(0, f; \Delta t, 0)$, respectively, w.r.t. the time separation variable Δt. Analogously, the TV average delay $B_{R_H}^{(1)}(t)$ and the TV delay spread $B_{R_H}^{(2)}(t)$ can also be computed following this approach, but considering instead $R_H(t, 0; 0, \Delta f)$, $\dot{R}_H(t, 0; 0, \Delta f)$, and $\ddot{R}_H(t, 0; 0, \Delta f)$ (the derivatives are w.r.t. the frequency lag variable Δf) in (12) and (13), and setting $\Delta f = 0$.

B. Consistency Analysis

According to [10], a non-stationary multipath channel model is consistent w.r.t. the:

 i) Average Doppler shift if $B_{\nu}^{(1)}(f) = B_{R_H}^{(1)}(f)$, $\forall f$
 ii) Doppler spread if $B_{\nu}^{(2)}(f) = B_{R_H}^{(2)}(f)$, $\forall f$
 iii) Average delay if $B_{\tau}^{(1)}(t) = B_{R_H}^{(1)}(t)$, $\forall t$
 iv) Delay spread if $B_{\tau}^{(2)}(t) = B_{R_H}^{(2)}(t)$, $\forall t$

1) General Case: In this part of the paper, we present a comparison between the results obtained for $B_{\nu}^{(1)}(f)$, $B_{\nu}^{(2)}(f)$, $B_{\tau}^{(1)}(t)$, and $B_{\tau}^{(2)}(t)$ with those obtained for $B_{R_H}^{(1)}(f)$, $B_{R_H}^{(2)}(f)$, $B_{R_H}^{(1)}(t)$, and $B_{R_H}^{(2)}(t)$ with the purpose of evaluating the consistency of the M2M channel model proposed in [7]. Aiming at drawing conclusions that are not constrained to a particular scattering configuration, we consider a generic arrangement of the location of the IOs, as shown in Fig. 1. Furthermore, we will assume again that the AODs ϕ_T and AOAs ϕ_R follow arbitrary circular symmetric distributions denoted by $p_{\phi}^T(\phi_T)$ and $p_{\phi}^R(\phi_R)$, respectively.

For reasons of comparison, we have computed $R_H(0, f; \Delta t, 0)$, $\dot{R}_H(0, f; \Delta t, 0)$, and $\ddot{R}_H(0, f; \Delta t, 0)$, and after evaluating the results at $\Delta t = 0$, the average Doppler shift was found as

$$B_{R_H}^{(1)}(f) = \int_{-\pi}^{\pi} \int_{-\pi}^{\pi} f^D(f) p_{\phi}^T(\phi_T) p_{\phi}^R(\phi_R) d\phi_T d\phi_R. \quad (14)$$

This is the same result as in (10), meaning that $B_{\nu}^{(1)}(f) = B_{R_H}^{(1)}(f)$. Analogously, the Doppler spread $B_{R_H}^{(2)}(f)$ was found to be

$$B_{R_H}^{(2)}(f) = \left\{ \int_{-\pi}^{\pi} \int_{-\pi}^{\pi} \left[f^D(f) \right]^2 p_{\phi}^T(\phi_T) p_{\phi}^R(\phi_R) d\phi_T d\phi_R - \left[B_{R_H}^{(1)}(f) \right]^2 \right\}^{1/2}. \quad (15)$$

This agrees with the result for $B_{\nu}^{(2)}(f)$ in (11), i.e., $B_{\nu}^{(2)}(f) = B_{R_H}^{(2)}(f)$. Hence, from equations (14) and (15), we can conclude that the channel model meets the Conditions i and ii.

With the same token, the average delay $B_{R_H}^{(1)}(t)$ and the delay spread $B_{R_H}^{(2)}(t)$ are shown to be

The average delay is obtained using the factor $-1/2\pi j$.

consistent. Indeed, after substituting $R_H(t, 0; 0, \Delta f)$, $\dot{R}_H(t, 0; 0, \Delta f)$, and $\ddot{R}_H(t, 0; 0, \Delta f)$ in their analogous equations to (12) and (13), it is shown that $B_{R_H}^{(1)}(t) = B_{\tau}^{(1)}(t)$ and $B_{R_H}^{(2)}(t) = B_{\tau}^{(2)}(t)$ hold. In fact, these quantities have the same form as in (14) and (15), respectively, if we replace there f by t, ν by τ, and $f^D(f)$ by $\tau(t)$. Thus, we can conclude that the channel model also meets the Conditions iii–iv. In addition, it is important to note that not only the propagation delays $\tau_{\ell,m}(t)$ are TV, but also the average delay $B_{\tau}^{(1)}(t)$ and the delay spread $B_{\tau}^{(2)}(t)$. Similarly, the Doppler shift $f_{\ell,m}^D(f)$, the average Doppler shift $B_{\nu}^{(1)}(f)$ and the Doppler spread $B_{\nu}^{(2)}(f)$ are directly influenced by the frequency of the communication system.

2) Particular Case: Next, we analyze the spectral moments of $H(t; f)$ for the particular case of the geometrical two-rings scattering model presented in [9]. It is assumed that T_X and R_X are surrounded by a ring of IOs with radii $G_T(\phi_T) = r_T$ and $G_T(\phi_R) = r_R$, respectively. It is also assumed that $D \gg \max\{\| \hat{\mathbf{p}}_{\ell}^T \|, \| \hat{\mathbf{p}}_m^R \|\}$, such that the path length $\| \mathbf{p}_{\ell,m}^S \| = G_s(\phi_{\ell}^T, \phi_m^R)$ can be approximated by [7]

$$G_s(\phi_{\ell}^T, \phi_m^R) \approx \frac{1}{C} \Big[r_T + r_R + D - r_T \cos(\phi_{\ell}^T) + r_R \cos(\phi_m^R) \Big]. \quad (16)$$

The AOD ϕ_{ℓ}^T and the AOA ϕ_m^R follow the von Mises PDF

$$p_{\phi}^k(\phi_k) = \frac{\exp\{\kappa_k \cos(\phi_k - \mu_k)\}}{2\pi I_0(\kappa_k)}, \quad k \in \{T, R\} \quad (17)$$

where κ_k is known as the concentration parameter, μ_k denotes the mean of the distribution, and I_0 is the modified zeroth-order Bessel function of the first kind.

After substituting the PDF shown in (17) in the spectral moments presented in (10) and (11), we obtain——after some mathematical manipulations——the closed-form expressions of the average Doppler shift $B_y^{(1)}(f)$ and Doppler spread $B_y^{(2)}(f)$ presented in (18) and (19), respectively (see the beginning of the next page) for $y \in \{\nu, R_H\}$, in which M_i^k is a constant defined as

$$M_i^k = \frac{I_f(\kappa_k)}{I_0(\kappa_k)} \cos(f\mu_k - g\gamma_k)$$

for $i \in \{1, 2, 3, 4\}$, $f \in \{1, 2\}$, and $g \in \{0, 1, 2\}$. If $i = 1$, then $f = 1$ and $g = 0$; if $i = 2$, then $f = 1$ and $g = 1$; if $i = 3$, then $f = 2$ and $g = 0$; and if $i = 4$, then $f = 1$ and $g = 1$; where I_1 (I_2) is the first (second) order modified Bessel function of the first kind.

In the same way, after substituting the PDF presented in (17) in the analogous equations to (10) and (11) for the average delay $B_x^{(1)}(t)$ and the delay spread $B_x^{(2)}(t)$ for $x \in \{\tau, R_H\}$, after some mathematical calculations, we prove that the obtained results are given by (20) and

$$B_\nu^{(1)}(f) = \sum_{k \in \{T,R\}} f_{\max}^k M_2^k = B_{R_H}^{(1)}(f) \tag{18}$$

$$B_\nu^{(2)}(f) = \frac{1}{\sqrt{2}} \left\{ \sum_{k \in \{T,R\}} \left(f_{\max}^k\right)^2 \left[1 + M_4^k - [\cos(2(\mu_k - \gamma_k)) + 1] \left(\frac{I_1(\kappa_k)}{I_0(\kappa_k)}\right)^2 \right] \right\}^{1/2} = B_{R_H}^{(2)}(f) \tag{19}$$

$$B_\tau^{(1)}(t) = \frac{r_T + D + r_R}{C} + \sum_{k \in \{T,R\}} q_k \left[M_1^k + t \left(\frac{f_{\max}^k}{(f_c + f)}\right) M_2^k \right] = B_{R_H}^{(1)}(t) \tag{20}$$

$$B_\tau^{(2)}(t) = \left\{ \sum_{k=T,R} \left[\left(\frac{r_k}{\sqrt{2}C}\right)^2 \left[1 + M_3^k - 2\left(M_1^k\right)^2\right] + t\left(\frac{q_k r_k f_{\max}^k}{C(f_c + f)}\right) \left[(\cos(\gamma_k)(1 + M_3^k) - 2 M_1^k M_2^k)\right] \right] \right.$$

$$\left. + t^2 \left(\frac{r_k}{\sqrt{2}C}\right)^2 \left[1 + M_4^k - 2\left(M_2^k\right)^2\right] \right\}^{1/2} = B_{R_H}^{(2)}(t) \tag{21}$$

---

(21), respectively (see the top of the next page), where $q_T = +1$ and $q_R = -1$.

IV. NUMERICAL RESULTS

Here, we compare the closed-form expressions of the spectral moments obtained from the FV Doppler shift $f_{\ell,m}^D(f)$ in (3) and the TV propagation delays $\tau_{\ell,m}(t)$ in (6) (see (18)-(21)) with the expressions of the spectral moments computed by means of the TF-CF in (7) (see (12) and (13)) when ϕ_T and ϕ_R follow the von Mises distribution. We take into account the parameters given in the IEEE 802.11p standard which has been drawn up for vehicular communications. We simulate the transmission of a data frame of duration $T_0 = 3.2$ ms (comprising 5×10^4 data symbols without considering the cyclic prefix) at a carrier frequency of $f_c = 5.9$ GHz and a system bandwidth of $B = 10$ MHz. We assume that the MSs are approaching along nearly parallel trajectories as presented in [7, Sec. IV.C], where $\gamma_T = 60°$, $\gamma_R = 250°$, $D = 500$ m, $r_T = 30$ m, $r_R = 30$ m, $f_{\max}^T = 500$ Hz, and $f_{\max}^R = 500$ Hz. We analyze four different scenarios assuming $\mu_T = 60°$ and $\mu_T = 120°$: Scenario 1 corresponds to an isotropic scattering condition with $\kappa_T = 0$ and $\kappa_R = 0$; while the other scenarios are designed to study non-isotropic scattering conditions with $\kappa_T = 1$, $\kappa_R = 10$ (Scenario 2), $\kappa_T = 10$, $\kappa_R = 1$ (Scenario 3), and $\kappa_T = 10$, $\kappa_R = 10$ (Scenario 4). The obtained graphs for each spectral moment considering the mentioned scenarios are presented in Figs. 2–5.

In Figs. 2 and 3, the FV average Doppler shift $B_y^{(1)}(f)$ and the FV Doppler spread $B_y^{(2)}(f)$ for $y \in \{\nu, R_H\}$, are illustrated, respectively. In these figures, we can see that the spectral moments remain almost constant regardless of their frequency dependence. This occurs because in vehicular communication systems based on the IEEE 802.11p standard, we have $f \ll f_c$. Thus, the contribution of the factor $(f_c + f)/f_c$ on the Doppler shift
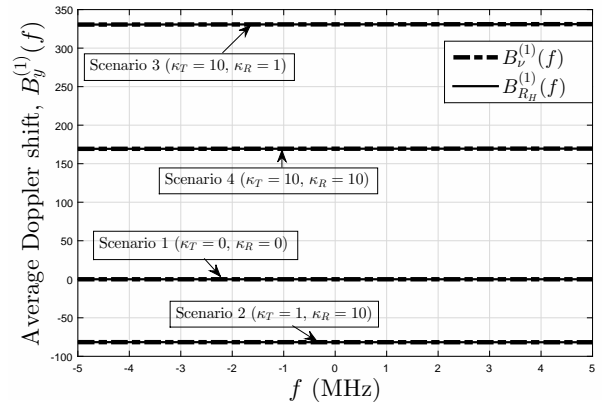

Fig. 2. FV average Doppler shift $B_y^{(1)}(f)$ for $y \in \{\nu, R_H\}$ and $B = 10$ MHz.

$f_{\ell,m}^D(f)$ in (3) is close to one. Furthermore, in Fig. 3, we can observe that the Doppler spread associated with Scenarios 2 and 3 are superimposed. Moreover, from the Fig. 2 and 3, we can see that the model is consistent according to the underlying criteria determined by the Conditions i and ii because $B_\nu^{(1)}(f) = B_{R_H}^{(1)}(f)$ and $B_\nu^{(2)}(f) = B_{R_H}^{(2)}(f)$.

Additionally, in Figs. 4 and 5, we present the obtained TV average delay $B_x^{(1)}(t)$ and the TV delay spread $B_x^{(2)}(t)$, respectively for $x \in \{\tau, R_H\}$. These figures reveal that the average delay and the delay spread are time-dependent, confirming that the proposed channel model in [7] and its spectral characteristics derived herein capture the non-stationarity of the physical channel. In addition, we can observe a perfect match between $B_\tau^{(1)}(t)$ and $B_{R_H}^{(1)}(t)$, and between $B_\tau^{(2)}(t)$ and $B_{R_H}^{(2)}(t)$. Therefore, the channel model fulfills the consistency criteria according to the Conditions iii and iv.
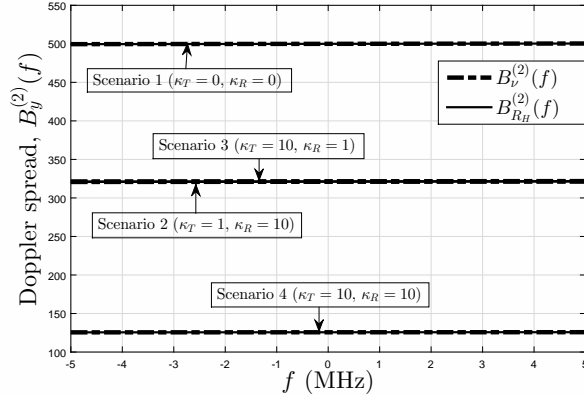
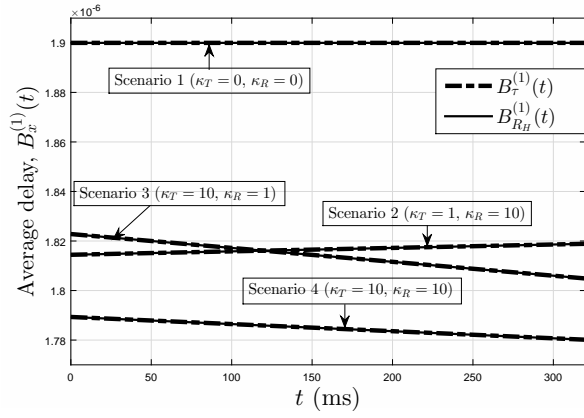Fig. 3. FV Doppler spread $B_y^{(2)}(f)$ for $y \in \{\nu, R_H\}$ and $B = 10$ MHz.

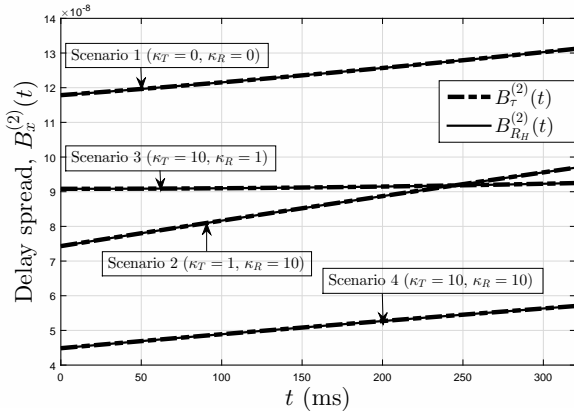Fig. 4. TV average delay $B_x^{(1)}(t)$ for $x \in \{\tau, R_H\}$.

Fig. 5. TV delay spread $B_x^{(2)}(t)$ for $x \in \{\tau, R_H\}$.

V. CONCLUSIONS

In this paper, we have derived general analytical expressions for the FV average Doppler shift, the FV Doppler spread, the TV average delay, and the TV delay spread of a novel non-WSSUS M2M double-Rayleigh

fading channel model. The obtained expressions have shown that the average delay and delay spread are TV quantities, which is in line with the reference GBSM for M2M double-Rayleigh fading channels, where the propagation delays are modeled by TV quantities. Moreover, the average Doppler shift and the Doppler spread are not only dependent on the carrier frequency, but also on the frequency of the communication system. If the system frequency is much smaller than the carrier frequency, the frequency dependence is almost negligible as it is assumed in several research works. However, if the system frequency is close to or equal to the carrier frequency, the frequency impact on the average Doppler shift and the Doppler spread becomes more evident and cannot be neglected. Finally, the results have shown the physical soundness of the reference GBSM for M2M double-Rayleigh fading channels because it fulfills all the conditions to be considered as consistent w.r.t. the spectral moments. Further research is needed to validate the theoretical results presented herein against measured data of real-world channels.

REFERENCES

[1] P. Hoeher, "A statistical discrete-time model for the WSSUS multipath channel," *IEEE Transactions on Vehicular Technology*, vol. 41, no. 4, pp. 461–468, Nov. 1992.

[2] A. G. Zajić, G. L. Stüber, T. G. Pratt, and S. T. Nguyen, "Wideband MIMO mobile-to-mobile channels: Geometry-based statistical modeling with experimental verification," *IEEE Transactions on Vehicular Technology*, vol. 58, no. 2, pp. 517–534, Feb. 2009.

[3] D. W. Matolak and J. Frolik, "Worse-than-Rayleigh fading: Experimental results and theoretical models," *IEEE Communications Magazine*, vol. 49, no. 4, pp. 140–146, Apr. 2011.

[4] L. Bernadó, T. Zemen, F. Tufvesson, A. F. Molisch, and C. F. Mecklenbrauker, "Delay and Doppler spreads of nonstationary vehicular channels for safety-relevant scenarios," *IEEE Transactions on Vehicular Technology*, vol. 63, no. 1, pp. 82–93, Jan. 2014.

[5] ——, "The (in-) validity of the WSSUS assumption in vehicular radio channels," in *Proc. 2012 IEEE 23rd International Symposium on Personal, Indoor and Mobile Radio Communications - (PIMRC)*, Sep. 2012, pp. 1757–1762.

[6] J. Karedal *et al.*, "A geometry-based stochastic MIMO model for vehicle-to-vehicle communications," *IEEE Transactions on Wireless Communications*, vol. 8, no. 7, pp. 3646–3657, Jul. 2009.

[7] C. A. Gutiérrez, J. J. Jaime-Rodríguez, J. M. Luna-Rivera, D. U. Campos-Delgado, and J. Vázquez-Castillo, "Modeling of non-WSSUS double-Rayleigh fading channels for vehicular communications," *Wireless Communications and Mobile Computing*, vol. 2017, 2017, in press.

[8] J. J. Jaime-Rodrguez, C. A. Gutirrez, D. U. Campos-Delgado, and J. M. Luna-Rivera, "First-order statistics analysis of two new geometrical models for non-WSSUS mobile-to-mobile channels," in *Proc. 2016 IEEE 12th International Conference on Wireless and Mobile Computing, Networking and Communications (WiMob)*, Oct. 2016, pp. 1–8.

[9] M. Pätzold, B. O. Hogstad, and N. Youssef, "Modeling, analysis, and simulation of MIMO mobile-to-mobile fading channels," vol. 7, no. 2, pp. 510–520, Feb. 2008.

[10] M. Pätzold, C. A. Gutiérrez, and N. Youssef, "On the consistency of non-stationary multipath fading channels with respect to the average Doppler shift and the Doppler spread," in *Proc. 2017 IEEE Wireless Communications and Networking Conference (WCNC'17)*, Mar. 2017.